Composite Hardening Effect in KNN Piezoelectric Ceramics

Haofeng Huang and Ke Wang *

Posted Date: 4 November 2024

doi: 10.20944/preprints202411.0200.v1

Keywords: $(K,Na)NbO_3$; ZnO; Lead-free piezoelectric ceramics; Mechanical quality factor Q_m; 0-3 composite material

Article

Composite Hardening Effect in KNN Piezoelectric Ceramics

Haofeng Huang and Ke Wang *

School of Materials Science and Engineering, Tsinghua University, Haidian District, Tsinghua Yuan, Beijing 100084, China; hhf22@mails.tsinghua.edu.cn

* Correspondence: wang-ke@tsinghua.edu.cn

Abstract: This study investigates the preparation of KNN-ZnO composites through optimized sintering conditions under both inert and oxygen atmospheres. Initial experiments employing inert hot pressing were hindered by the necessity for annealing, which resulted in cracks due to the differing thermal expansion coefficients of KNN and ZnO, rendering this method unsuitable for composite fabrication. Consequently, sintering under an oxygen atmosphere was adopted, yielding a uniform distribution of ZnO particles within the KNN matrix. The resultant microstructure demonstrated significant densification, enhanced homogeneity, and minimal porosity. Electrical performance evaluations revealed that while the incorporation of ZnO led to a slight reduction in the ferroelectric properties (d_{33} and polarization) of the KNN matrix, it concurrently improved the electromechanical quality factor (Q_m) by 40%. However, the overall enhancements were less pronounced when compared to analogous BNT-BT systems, underscoring the necessity for further optimization of processing conditions to boost electromechanical efficiency and piezoelectric response in KNN-based ceramics.

Keywords: (K,Na)NbO_3; ZnO; Lead-free piezoelectric ceramics; Mechanical quality factor Q_m; 0-3 composite material

1. Introduction

Piezoelectric ceramics are commonly tailored to suit various application scenarios, resulting in a classification into soft and hard piezoelectric ceramics based on specific parameter values. Soft piezoelectric ceramics are characterized by elevated piezoelectric constants (e.g., d_{33}), high electromechanical coupling coefficients (e.g., k_p), and notable dielectric loss (tanδ), alongside a reduced coercive field (E_c) and mechanical quality factor (Q_m). These properties make them particularly suitable for applications such as ultrasonic atomization, remote sensing, and medical diagnostics. Conversely, hard piezoelectric ceramics are defined by their high mechanical quality factor (Q_m) and low dielectric loss (tanδ), rendering them ideal for applications that demand high power output and efficient energy conversion. In high-power ultrasonic systems—such as those used in cutting, cleaning, and welding—hard piezoelectric ceramics play a critical role in ensuring system efficiency and stability. Their capabilities are especially vital in industrial and medical sectors where significant energy output is essential.

The hardening effect of PZT is typically achieved through acceptor doping, involving the substitution of Pb^{2+} with Na^+ or Ti^{4+} with Fe^{3+} or Ni^{2+}. Currently, three mechanisms are proposed to elucidate the hardening effect of PZT [1], as illustrated in Figure 1: the bulk effect, domain-wall effect, and surface effect. In the bulk effect, positively charged oxygen vacancies are generated in acceptor-doped PZT to compensate for the negatively charged acceptor centers, resulting in the formation of "defect associations." These associations restrict domain wall movement and stabilize the domain structure, as shown in Figure 1(b). The domain-wall effect, on the other hand, describes the migration of defects, such as oxygen vacancies, to the domain walls over time, thereby creating pinning centers that impede domain wall movement, as depicted in Figure 1(c). The surface effect involves the diffusion of charged carriers towards the boundaries of the microstructure to counteract

 doi:10.20944/preprints202411.0200.v1

depolarization fields, which generates clamping forces that further limit domain wall movement, as illustrated in Figure 1(d). Each of these mechanisms possesses unique applications, and determining their relative effectiveness remains challenging. Despite the established nature of PZT, its hardening mechanisms are not yet fully understood. The subsequent sections will address the control of hardening effect through doping in KNN.

Similar to PZT, the hardening effect of KNN predominantly depends on acceptor doping, with dopants including Cu^{2+} and its compounds, such as CuO, $K_4CuNb_8O_{23}$ (KCN), and $K_{5.4}Cu_{1.3}Ta_{10}O_{29}$ (KCT). The variations in the mechanical quality factor (Q_m) of doped KNN are illustrated in Figure 2, with a summary of the data presented in Table 1. The hardening mechanisms of KNN are largely analogous to those of PZT, primarily encompassing the bulk effect and domain-wall effect; however, they do not fully account for all experimental observations, necessitating further investigation [1]. As shown in Table 1, the Q_m of hardened KNN doped with CuO or KCT+CuO reaches 2500 and 3000, respectively, surpassing that of hard PZT, which is 2000. Nonetheless, the d_{33} value of hardened KNN remains below 100, significantly lower than the 265 of hard PZT, which constrains its industrial applicability. Therefore, it is imperative to design KNN-based piezoelectric ceramics with improved overall performance. To this end, researchers have proposed ceramic composite systems to facilitate hardening effect control.

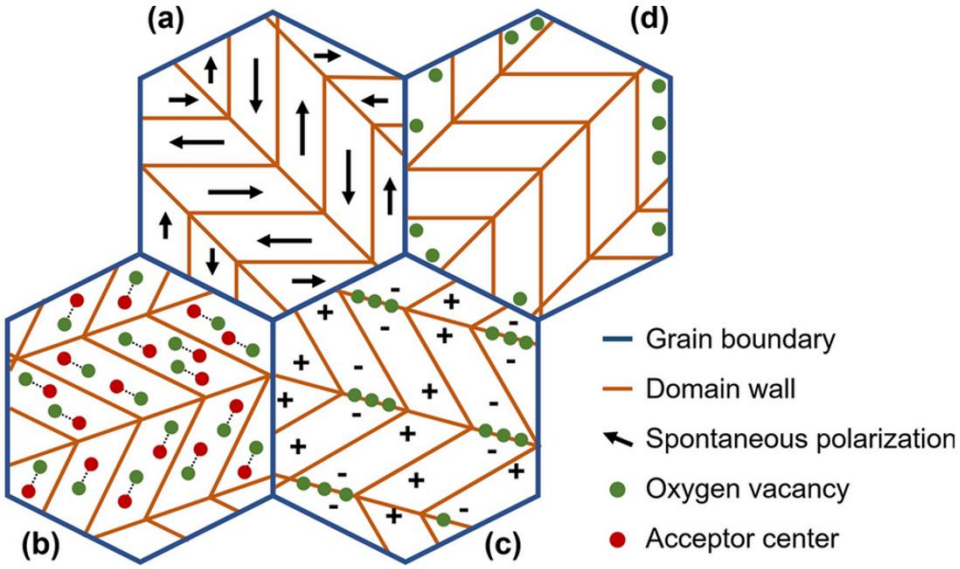

Figure 1. Models of the three distinct hardening mechanisms in PZT [1]: (a) multiple domains within a single grain; (b) bulk effect; (c) domain-wall effect; (d) surface effect.

Preprints.org (www.preprints.org) | NOT PEER-REVIEWED | Posted: 4 November 2024 doi:10.20944/preprints202411.0200.v1

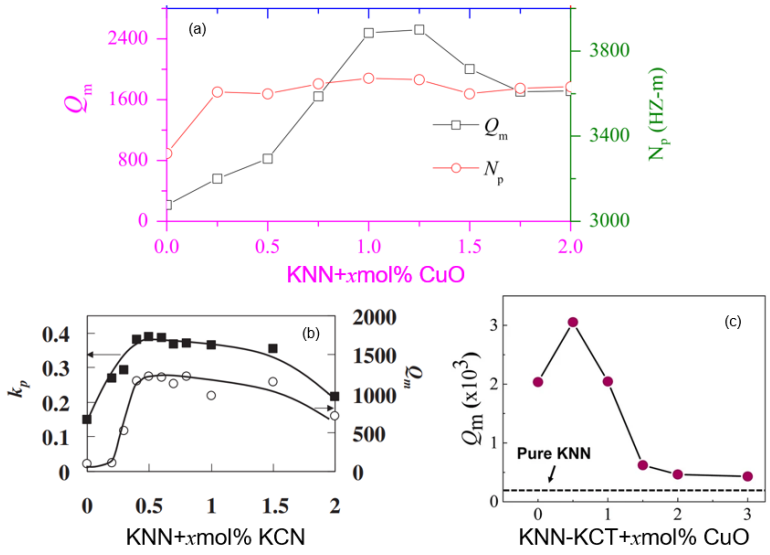

Figure 2. Q_m of KNN with different dopants: (a) KNN + x mol% CuO [3]; (b) KNN + x mol% KCN [4]; (c) KNN-KCT + x mol% CuO [2,5].

Table 1. Performance data of different piezoelectric ceramics.

Materials	Type	d_{33}(pC/N)	Q_m	Ref.
Soft PZT	Soft	500	100	[6,8]
Hard PZT	Hard	265	2000	[6,8]
KNN	——	108	176	[7]
KNN+CuO	Hard	82	2523	[3]
KNN+KCN	Hard	——	1200	[4]
KNN+KCT+CuO	Hard	94	3053	[5]

The BNT-BT-ZnO composite material was developed to tackle the issue of thermal depolarization in the BNT-BT system. A study by Zhang in 2015 demonstrated that ZnO effectively delays the depolarization temperature, whereas ZrO_2 does not exhibit a similar effect, underscoring the distinctive properties of ZnO [9]. In this composite, ZnO particles are situated at the grain boundaries of BNT-BT, forming a 0-3 type composite material, as illustrated in Figure 3. Several models have been proposed to elucidate the mechanism behind depolarization suppression in BNT-BT-ZnO composites, including the "charge compensation model," the "pinning effect of ZnO on nanoscale ferroelectric domains" [10], the "thermal stress-induced ferroelectric phase stability" model [11], and the model concerning Zn incorporation into the lattice [12]. All these models relate to the enhanced stability of ferroelectric domains and phases, which contribute to an increase in the mechanical quality factor (Q_m). Thus, linking the suppression of thermal depolarization to the enhanccement of Q_m represents an innovative approach.

In 2017, it was observed that the hardening effect of the BNT-BT-ZnO composite system was significantly enhanced, with Q_m increasing in proportion to the ZnO content, as depicted in Figure 3 [13]. While the aforementioned models can account for the increase in Q_m with higher ZnO content, they fail to explain the subsequent decrease in Q_m when ZnO content is further increased. Consequently, a clamping effect due to strain incompatibility caused by ZnO was proposed, as shown in Figure 3 [13]. Given the inferior piezoelectric response of ZnO compared to the BNT-BT matrix, the strain in the two phases becomes inconsistent, necessitating that the matrix accommodate the

 doi:10.20944/preprints202411.0200.v1

strain of ZnO. This accommodation leads to restricted matrix strain, reduced domain switching losses, and an increase in Q_m. However, excessive clamping can elevate domain wall density, resulting in higher energy loss and a decrease in Q_m. This model thus presents a competitive mechanism whereby ZnO limits the matrix strain without excessive clamping, thereby preventing undue stress and a high domain wall density in the matrix. Ultimately, an optimal Q_m can be attained by identifying the best compositional balance.

Previous research has introduced BNT-BT-ZnO composites and their hardening performance regulation, with analogous studies being applied to the KNN system. Some researchers have attempted to develop KNN-ZnO composites [14], as shown in Figure 3, which includes SEM images and elemental distribution. The density of ZnO is reported as 5.60 g/cm³, while the theoretical density of pure KNN is 4.51 g/cm³. In this study, the density of pure KNN was relatively low, measured at only 4.00 g/cm³, indicating a densification of less than 90%. Although the density of KNN-ZnO increased with higher ZnO content, the overall density level remained suboptimal [14]. This study primarily explored the properties of KNN-ZnO composites, such as the temperature stability of d_{33}, while the investigation of hardening performance has yet to be addressed. The present work aims to fill this gap.

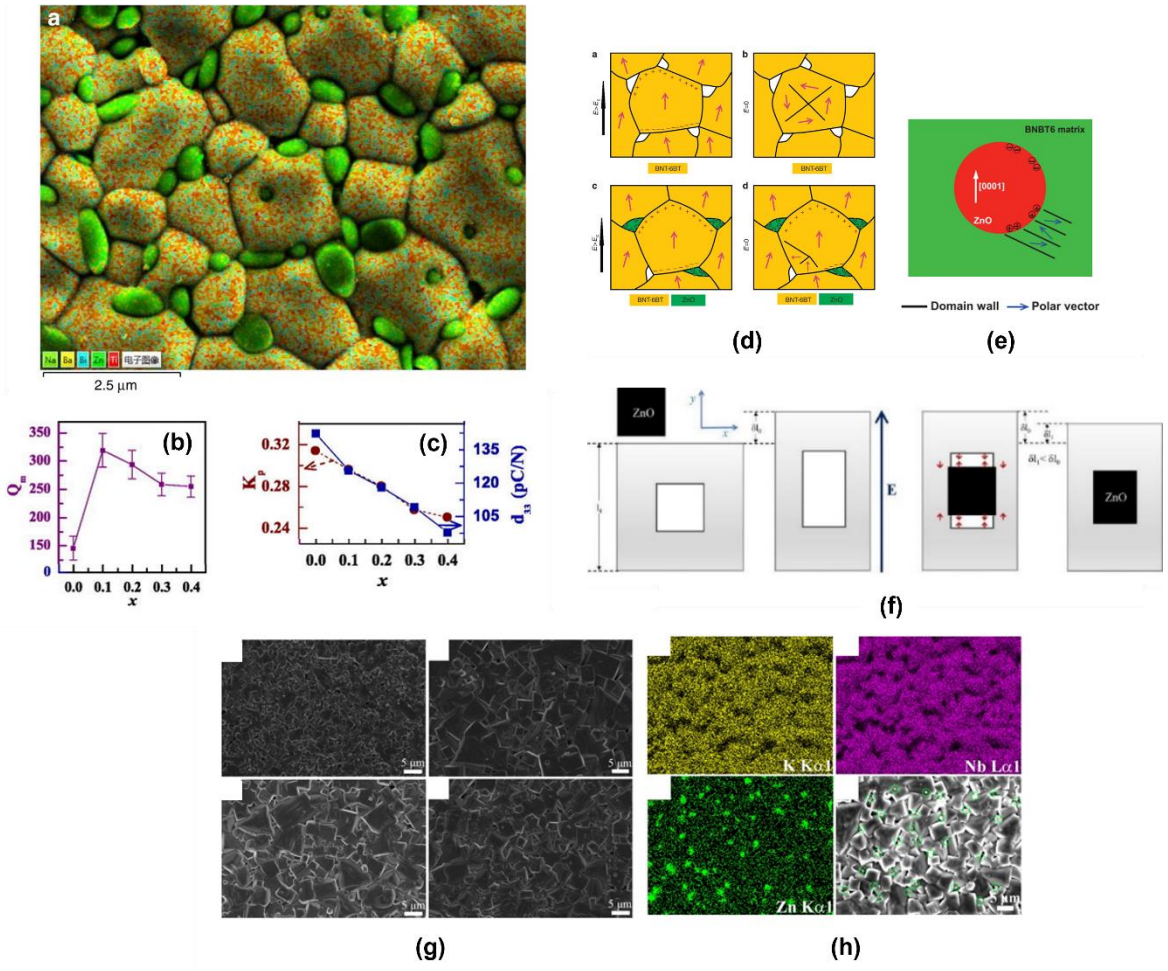

Figure 3. (a) SEM elemental distribution of BNT-BT-30 mol% ZnO composite; (b) and (c) variations of the mechanical quality factor Q_m, electromechanical coupling coefficient k_p, and piezoelectric constant d_{33} with composition in BNT-BT-xZnO (where x represents molar fraction, e.g., x=0.1 indicates 10 mol%); (d) charge compensation model; (e) ZnO pinning of nanoscale ferroelectric domains; (f) clamping effect; (g) SEM and (h) elemental distribution of KNN-20 mol% ZnO composite.

 doi:10.20944/preprints202411.0200.v1

2. Results and Discussion

The SEM pictures of KNN-ZnO composites prepared by hot pressing under an inert atmosphere are presented in Figure 4. In these images, ZnO particles appear as white spots, uniformly distributed within the KNN matrix. Each sub-figure highlights the ZnO particles with red circles for clarity. It is evident that, with increasing ZnO content, both the number and distribution density of the white particles (ZnO) increase correspondingly, aligning with theoretical expectations. Additionally, the higher ZnO content is associated with an increased pore density, which may be attributed to the mismatch in thermal expansion coefficients between ZnO and KNN during the annealing process, resulting in crack formation at the interface.

To confirm that the white spots observed in Figure 4 are indeed ZnO particles, energy dispersive X-ray spectroscopy (EDS) was conducted on the same region, specifically analyzing the Zn element, as shown in Figure 4. The upper images in Figure 4 correspond to the images below. Initially, a secondary electron image was obtained, followed by EDS scanning of the same area, resulting in a continuous dataset of secondary electron and EDS images. The red circles in Figure 4 indicate the corresponding locations in both the secondary electron and EDS images, confirming that the white spots are regions enriched in Zn content, thereby validating their identification as ZnO particles.

To distinctly differentiate between ZnO and KNN in the material, backscattered electron (BSD) images were acquired, as shown in Figure 4. According to the literature [15], the backscattering coefficients of the different phases were calculated, with higher backscattering coefficients producing brighter areas in the BSD images. The backscattering coefficient of ZnO is slightly higher than that of KNN, resulting in bright white regions in Figure 4 corresponding to the ZnO phase, gray regions representing the KNN matrix, and black regions indicating pores. Compared to the secondary electron images, BSD images demonstrate superior contrast, facilitating a clearer distinction between the ZnO and KNN phases.

From the images, it is apparent that as the ZnO content increases, the total area of the white regions (ZnO phase) also increases in accordance with expectations. Furthermore, the density of the black regions (pores) significantly rises with increased ZnO content. This phenomenon may arise from the thermal expansion mismatch between ZnO and KNN during annealing, or it may be attributed to the enhanced sintering aid effect of ZnO, which, at higher contents, results in an excessive liquid phase formation during hot pressing, ultimately leading to pore formation.

Based on the SEM images, the microstructure of the KNN-ZnO composite prepared in this study markedly differs from that of the BNT-BT-ZnO composite reported in the literature. In this work, KNN grains exhibited rapid growth, resulting in larger grain sizes that partially engulf small ZnO particles, leading to a microstructure in which KNN grains encapsulate ZnO particles. Conversely, the literature describes the BNT-BT-ZnO composite with ZnO particles uniformly distributed along the grain boundaries. These distinct microstructures contribute to differences in the internal stress distribution within the material.

The encapsulation of ZnO particles by KNN grains may lead to a more complex stress distribution during the sintering process, whereas the literature-reported structure, with ZnO uniformly distributed at the grain boundaries, facilitates a more homogeneous stress distribution. Consequently, to achieve a structure where ZnO is uniformly distributed at the grain boundaries, as noted in the literature, it is essential to adjust the sintering conditions to inhibit excessive KNN grain growth, promoting a more uniform distribution of ZnO.

 doi:10.20944/preprints202411.0200.v1

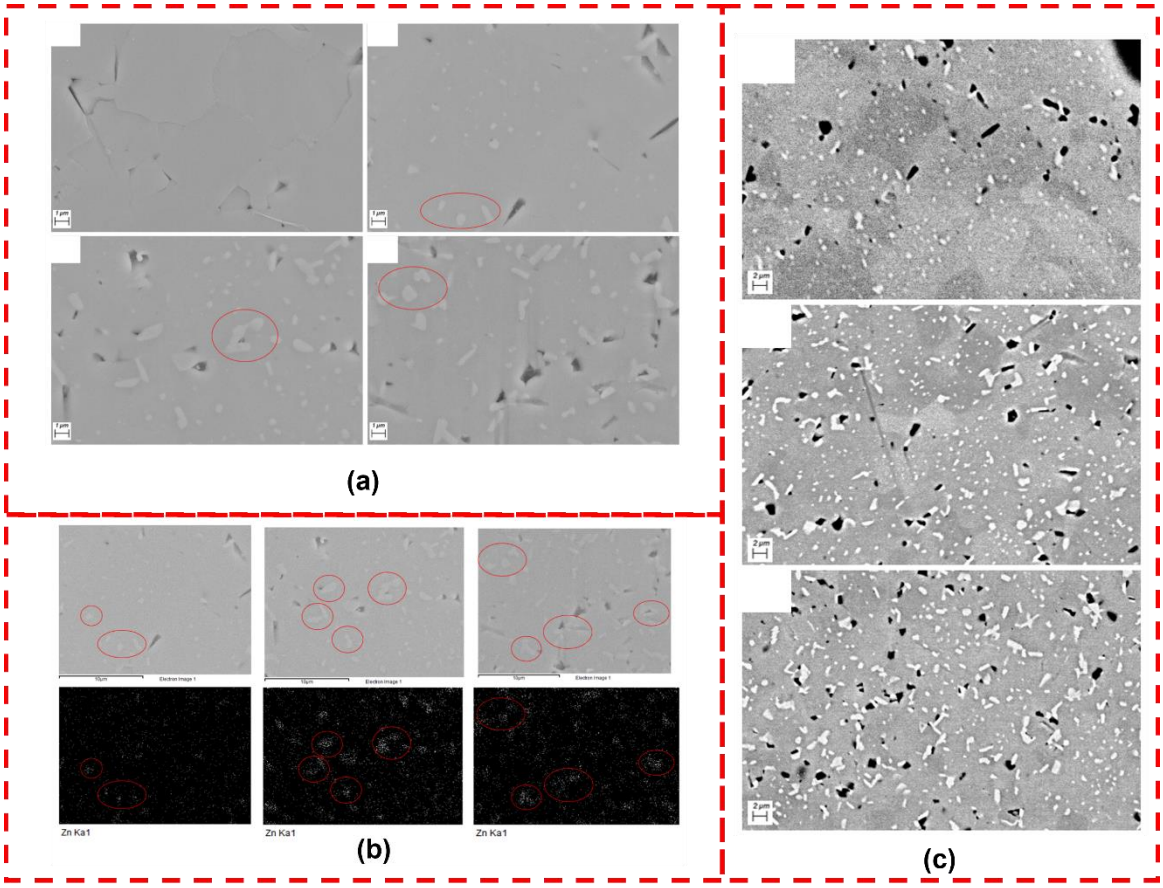

Figure 4. (a) Secondary electron image; (b) distribution of the Zn; (c) backscattered electron (BSD) image.

To achieve this objective, the study made specific adjustments to the sintering conditions, including optimizing the sintering temperature and time to suppress KNN grain growth, thereby obtaining a microstructure more aligned with that reported in the literature. Following these optimizations, SEM images were captured, as shown in Figure 5, demonstrating that the distribution of ZnO particles in the optimized material is more uniform, and the size of KNN grains has decreased, aligning more closely with the literature description.

As illustrated in Figure 5, although the optimized sintering conditions successfully produced a composite structure with ZnO particles uniformly distributed among KNN grains, several significant issues arose post-annealing. The disparity in thermal expansion coefficients between KNN and ZnO resulted in the formation of numerous microcracks within the material upon cooling to room temperature. Some cracks even manifested as visible fractures at the sample edges. This observation indicates that while hot pressing in an inert atmosphere effectively promotes the integration of ZnO and KNN, the thermal expansion mismatch during annealing induces considerable internal stress, ultimately resulting in microcrack and fracture formation.

These findings highlight the limitations of hot pressing under inert conditions for preparing composite materials, particularly those requiring subsequent annealing. While the annealing step aims to enhance the microstructure and reduce defects, the thermal expansion mismatch between KNN and ZnO phases renders annealing a critical factor that adversely impacts the structural integrity of the material, leading to reduced mechanical stability.

 doi:10.20944/preprints202411.0200.v1

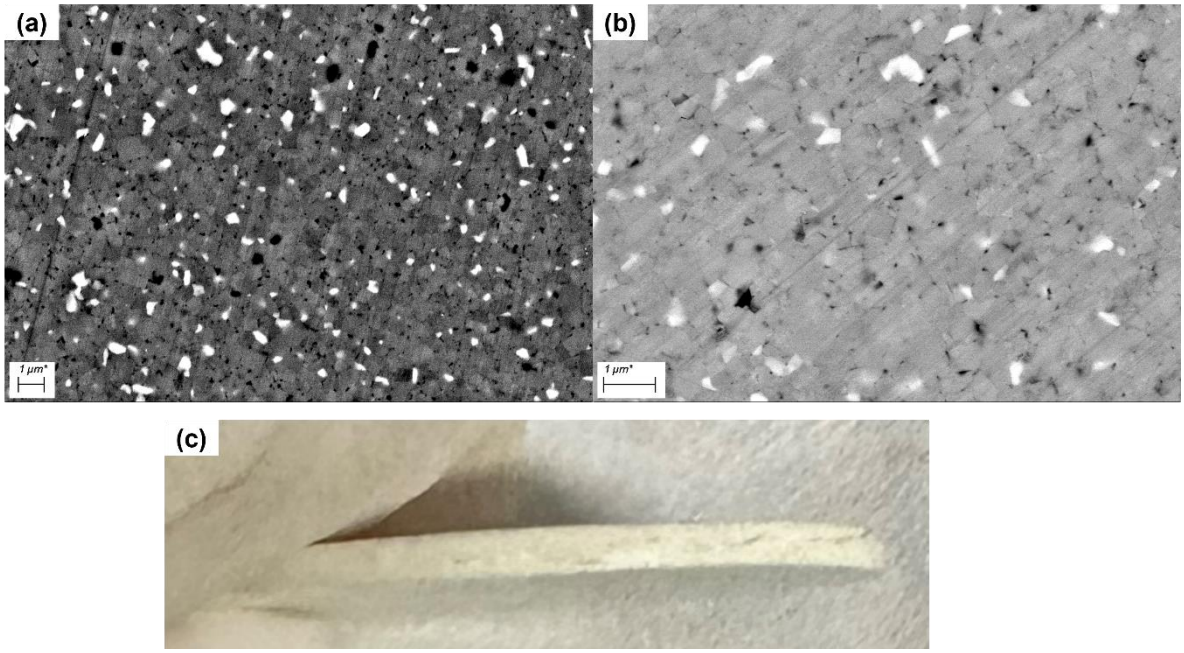

Figure 5. (a) Backscattered electron image; (b) secondary electron image; (c) cracks observed in the sample after annealing.

To mitigate the impact of the annealing step, this study further explored hot pressing in an oxygen atmosphere while strictly controlling sintering conditions to inhibit KNN grain growth, aiming to fabricate KNN-ZnO composites with improved structure and density. The SEM images of the sintered samples are presented in Figure 6, with Figure 6(a) displaying the secondary electron image and Figure 6(b) showing the backscattered electron image.

As depicted in Figure 6, hot pressing in an oxygen atmosphere, combined with optimized sintering parameters, successfully yielded a KNN-ZnO composite with a structure analogous to that described in the literature. ZnO particles were uniformly distributed among KNN grains, and KNN grain growth was effectively suppressed, resulting in significantly smaller grain sizes and a uniform overall structure. Additionally, the backscattered electron image reveals a very high density with almost no pores, indicating a substantial improvement in material densification through the hot pressing process in an oxygen atmosphere.

These results suggest that employing hot pressing in an oxygen atmosphere not only effectively circumvents the issues associated with the annealing step but also markedly enhances the quality of the composite's microstructure, yielding a more uniform distribution of KNN grains and ZnO particles, further increasing the density and structural integrity of the composite material.

Subsequent electrical performance testing was conducted on the prepared KNN-ZnO composite, including assessments of ferroelectric hysteresis loops, piezoelectric constant (d_{33}), and impedance spectroscopy. The results, presented in Figure 6, indicate that the ferroelectric hysteresis loops of the composite material exhibited a decrease in maximum polarization, remnant polarization, and coercive field compared to pure KNN. This reduction can be attributed to the incorporation of ZnO, a non-ferroelectric heterogeneous phase, into the KNN matrix, which diminishes the overall ferroelectric properties and weakens polarization characteristics.

Furthermore, the testing results for d_{33}, electromechanical quality factor (Q_m), and maximum phase angle are summarized in Table 2. Compared to pure KNN, the d_{33} and maximum phase angle of the ZnO-composited samples decreased to varying extents, while the Q_m value increased by 40%. Despite this enhancement, the overall Q_m remains relatively low, suggesting that while the introduction of ZnO has improved the electromechanical quality factor to some degree, the extent of enhancement is still less significant than that observed in the BNT-BT system reported in the literature. This may be linked to the properties of the matrix material; the BNT matrix, as noted in the literature, possesses a higher Young's modulus than KNN, potentially resulting in more pronounced

 doi:10.20944/preprints202411.0200.v1

modification effects when combined with ZnO, thereby exhibiting greater improvements in electrical performance.

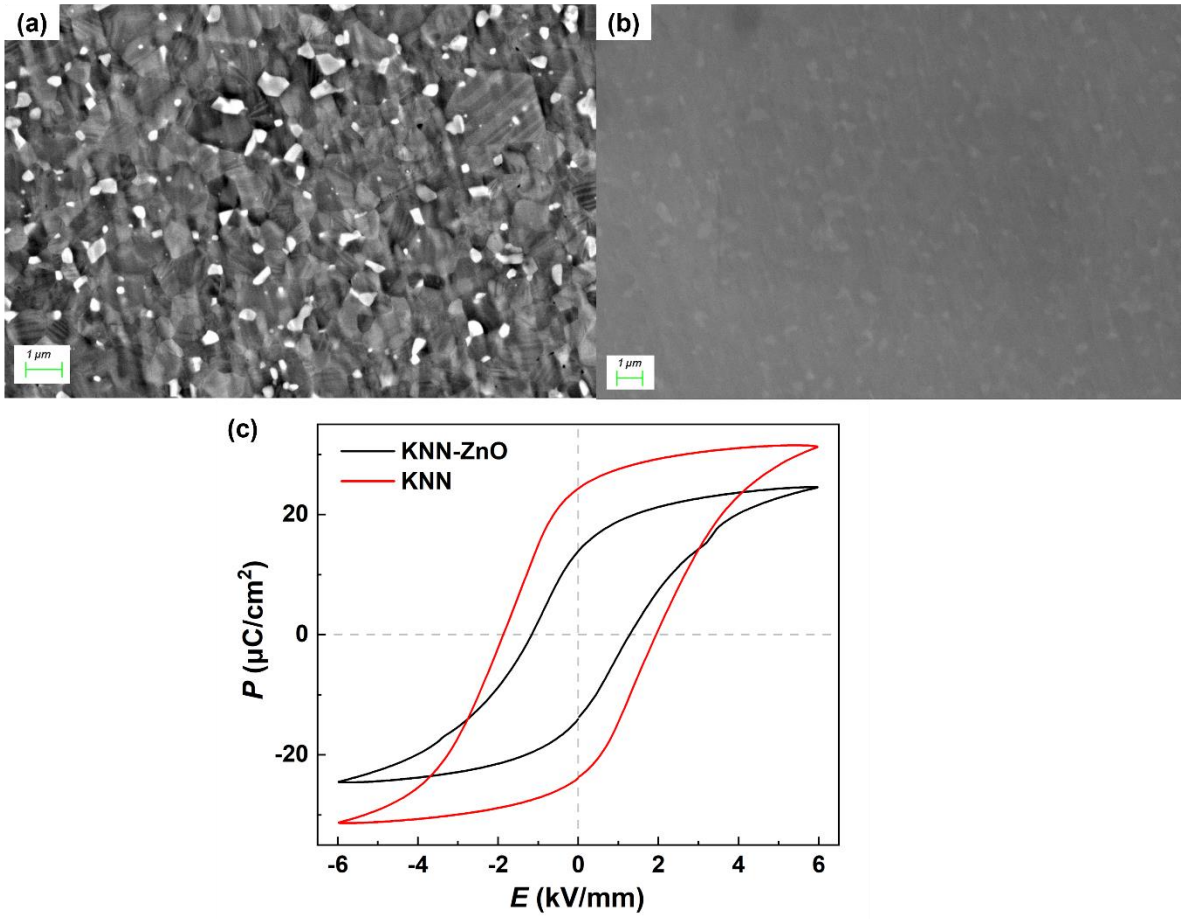

Figure 6. (a) Secondary electron image; (b) backscattered electron image; (c) ferroelectric hysteresis loop.

Table 2. Electrical Properties of KNN-ZnO.

Materials	P_r (μC/cm²)	P_{max} (μC/cm²)	E_c+ (kV/mm)	E_c- (kV/mm)	d_{33} (pC/N)	Q_m	Phase angle(°)
KNN	24.3	31.3	1.94	-1.86	112±6	71±30	68±5
KNN-20mol%ZnO	13.9	24.5	1.29	-1.15	90±10	106±10	60±8

3. Conclusions

In conclusion, this study demonstrates the successful preparation of KNN-ZnO composites through the optimization of sintering conditions under both inert and oxygen atmospheres. Initial attempts at inert hot pressing were hindered by the formation of cracks due to the thermal expansion mismatch between KNN and ZnO, rendering this method unsuitable for effective composite formation. In contrast, sintering under an oxygen atmosphere facilitated a uniform distribution of ZnO particles within the KNN matrix, resulting in a microstructure characterized by high densification, improved homogeneity, and minimal porosity.

While the introduction of ZnO led to a slight reduction in the ferroelectric properties of the KNN matrix, it notably enhanced the electromechanical quality factor (Q_m) by 40%. Despite these improvements, the overall performance enhancement was less pronounced compared to similar

 doi:10.20944/preprints202411.0200.v1

BNT-BT systems. This indicates that further optimization of processing conditions and composite composition is essential to maximize the electromechanical efficiency and piezoelectric response of KNN-based ceramics. Future work should focus on refining these parameters to achieve a balanced enhancement in both mechanical and electrical properties.

4. Experimental

The preparation of KNN powder commenced with batching a total powder weight of 60 grams per ball mill jar, with four jars prepared in total. The raw powders were mixed and placed into the ball mill jars, followed by the addition of ethanol. The mixture underwent an initial ball milling process for 24 hours. After milling, the slurry was dried and subjected to preliminary calcination to obtain the perovskite phase of KNN. The calcined powder was then milled for an additional 24 hours, dried, and sieved through a 60-mesh sieve to yield the KNN powder.

Subsequently, KNN+xZnO powder was prepared using ZnO with a purity of 99%, purchased from Xianfeng Nano. The KNN powder was mixed with varying masses of ZnO. This mixed powder underwent a third round of ball milling for 24 hours, followed by drying and sieving through a 60-mesh sieve to produce the KNN+xZnO powder.

The KNN+xZnO powder was loaded into a hot-pressing mold and sintered under an inert atmosphere of argon. The resulting hot-pressed samples were cylindrical, with a diameter of approximately 24.5 mm and a thickness of about 4.3 mm, exhibiting a uniform black color attributed to carbonization from the graphite mold and oxygen deficiency during the sintering process. The formation of numerous oxygen vacancies contributed to the development of defect energy levels within the bandgap, enhancing light absorption and resulting in the black appearance of the samples.

The hot-pressed cylindrical samples were then cut into rectangular specimens measuring 6.5 × 6.5 × 1.5 mm, which also displayed a black color. These rectangular specimens underwent annealing in an air atmosphere to ensure adequate compensation of oxygen vacancies. To minimize the volatilization of alkali metal elements during annealing, the samples were embedded in corresponding powders.

Following annealing, the rectangular specimens were polished to a standard size of 6 × 6 × 1 mm. The annealed samples initially appeared white, with the color gradually darkening to yellow as the ZnO content increased. Silver electrodes were then applied to the surfaces of the specimens, and any residual silver on the edges was removed. The prepared samples were subsequently subjected to X-ray diffraction (XRD), scanning electron microscopy (SEM), and relevant electrical performance testing.

XRD analysis was conducted using a Rigaku model X-ray diffractometer. SEM characterization was performed with a ZEISS Merlin scanning electron microscope to observe the surface morphology and elemental distribution of the samples. Dielectric spectroscopy was tested using a TZDM model RT-800 and a Tonghui TH2827C Precision LCR Meter. Poling treatment was carried out with an ET2673D-4 piezoelectric ceramic high-voltage poling apparatus (Nanjing En Tai Electronic Instrument Co., Ltd.), applying a poling field of 3 kV/mm at 120 °C. The d33 values were measured using a ZJ-3A quasi-static d_{33} meter from the Chinese Academy of Sciences Institute of Acoustics. Ferroelectric hysteresis loops were recorded using a TF ANALYZER 1000 (aixACCT), and impedance analysis was conducted with a Tonghui TH2839 Impedance Analyzer.

References

1. Nguyen T N, Thong H C, Zhu Z X, et al. Hardening effect in lead-free piezoelectric ceramics[J]. Journal of Materials Research, 2021, 36(5): 996-1014.
2. B. Jaffe, R. S. Roth, and S. Marzullo. Piezoelectric Properties of Lead Zirconate - Lead Titanate Solid - Solution Ceramics[J]. Journal of Applied Physics, 1954, 25: 809-810.
3. Lin D, Kwok K W, Chan H L W. Piezoelectric and ferroelectric properties of Cu-doped $K_{0.5}Na_{0.5}NbO_3$ lead-free ceramics[J]. Journal of Physics D: Applied Physics, 2008, 41(4): 045401.
4. Matsubara M, Yamaguchi T, Kikuta K, et al. Sinterability and piezoelectric properties of (K, Na) NbO_3 ceramics with novel sintering aid[J]. Japanese Journal of Applied Physics, 2004, 43(10R): 7159.

 doi:10.20944/preprints202411.0200.v1

5. Park B C, Hong I K, Jang H D, et al. Highly enhanced mechanical quality factor in lead-free ($K_{0.5}Na_{0.5}$) NbO_3 piezoelectric ceramics by co-doping with $K_{5.4}Cu_{1.3}Ta_{10}O_{29}$ and CuO[J]. Materials Letters, 2010, 64(14): 1577-1579.
6. Tan Q, Li J, Viehland D. Role of lower valent substituent-oxygen vacancy complexes in polarization pinning in potassium-modified lead zirconate titanate[J]. Applied physics letters, 1999, 75(3): 418-420.
7. Zhang M H, Wang K, Du Y J, et al. High and temperature-insensitive piezoelectric strain in alkali niobate lead-free perovskite[J]. Journal of the American Chemical Society, 2017, 139(10): 3889-3895.
8. Gao Y, Uchino K, Viehland D. Time dependence of the mechanical quality factor in "hard" lead zirconate titanate ceramics: development of an internal dipolar field and high power origin[J]. Japanese journal of applied physics, 2006, 45(12R): 9119.
9. Zhang J, Pan Z, Guo F F, et al. Semiconductor/relaxor 0–3 type composites without thermal depolarization in $Bi_{0.5}Na_{0.5}TiO_3$-based lead-free piezoceramics[J]. Nature communications, 2015, 6(1): 1-10.
10. Fan Z, Zhou L, Kim T H, et al. Mechanisms of enhanced thermal stability of polarization in lead-free $(Bi_{1/2}Na_{1/2})_{0.94}Ba_{0.06}TiO_3$/ZnO ceramic composites[J]. Physical Review Materials, 2019, 3(2): 024402.
11. Riemer L M, Lalitha K V, Jiang X, et al. Stress-induced phase transition in lead-free relaxor ferroelectric composites[J]. Acta Materialia, 2017, 136: 271-280.
12. Mahajan A, Zhang H, Wu J, et al. Effect of phase transitions on thermal depoling in lead-free 0.94 ($Bi_{0.5}Na_{0.5}TiO_3$)–0.06 ($BaTiO_3$) based piezoelectrics[J]. The Journal of Physical Chemistry C, 2017, 121(10): 5709-5718.
13. KV L, Riemer L M, Koruza J, et al. Hardening of electromechanical properties in piezoceramics using a composite approach[J]. Applied Physics Letters, 2017, 111(2): 022905.
14. Pan Z, Chen J, Fan L, et al. Enhanced piezoelectric properties and thermal stability in the ($K_{0.5}Na_{0.5}$) NbO_3: ZnO lead-free piezoelectric composites[J]. Journal of the American Ceramic Society, 2015, 98(12): 3935-3941.
15. J. I. Goldstein et al. 张大同 译. 扫描电子显微技术与 X 射线显微分析[M]. 北京：科学出版社，1988.